ISSN 0016-7029, Geochemistry International, 2007, Vol. 45, No. 1, pp. 1–14. © Pleiades Publishing, Ltd., 2007.
Original Russian Text © S.V. Rasskazov, A.M. Il'yasova, A.A. Konev, T.A. Yasnygina, M.N. Maslovskaya, N.N. Fefelov, E.I. Demonterova, E.V. Saranina, 2007, published in Geokhimiya, 2007, No. 1, pp. 3–18.

Geochemical Evolution of the Zadoi Alkaline–Ultramafic Massif, Cis-Sayan Area, Southern Siberia

S. V. Rasskazov, A. M. Il'yasova, A. A. Konev, T. A. Yasnygina, M. N. Maslovskaya, N. N. Fefelov, E. I. Demonterova, and E. V. Saranina

Institute of the Earth's Crust, Siberian Division, Russian Academy of Sciences, ul. Lermontova 128, Irkutsk, 664033 Russia

e-mail: rassk@crust.irk.ru

Received March 21, 2005

Abstract—The unaltered magmatic rocks of the Zadoi Massif were analyzed for Sr isotopic composition and concentrations of major oxides and trace elements by ICP MS. The evolution of the massif involved four phases: (i) perovskite and ilmenite clinopyroxenites, (ii) ijolites, (iii) nepheline syenites, and (iv) carbonatites. The perovskite clinopyroxenites have anomalously high Ce/Pb (223–1132) and Pr/Sr × 1000 (70–360) ratios at a low initial Sr isotopic ratio $(^{87}Sr/^{86}Sr)_0$ = 0.70247–0.70285. The ilmenite clinopyroxenites have Ce/Pb and Pr/Sr × 1000 ratios approaching those in basalts of oceanic islands (OIB) (decreasing to 39 and 30, respectively) at a simultaneous increase in the $(^{87}Sr/^{86}Sr)_0$ ratios (0.7030–0.7036). The ijolites and nepheline syenites have patterns of incompatible trace elements similar to those in OIB and the highest $(^{87}Sr/^{86}Sr)_0$ ratios (0.70346–0.70414). The carbonatites are complementarily enriched in incompatible elements of the nepheline syenites and have $(^{87}Sr/^{86}Sr)_0$ = 0.7029–0.7034, which is comparable with the range of analogous ratios for the ilmenite clinopyroxenites. Our geochemical data indicate that the carbonatites were formed as an immiscible liquid or fluid, which separated from the ijolite–nepheline syenite melt during its interaction with the source material of the perovskite and ilmenite clinopyroxenites.

DOI: 10.1134/S0016702907010016

INTRODUCTION

One of the actively debated petrological issues is the genesis of alkaline–ultramafic complexes with carbonatites. The high alkalinity of rocks composing these complexes was often thought to have resulted from their secondary metasomatic recycling. Numerous experimental data and field observations suggest that carbonatites are formed with the participation of several processes, such as separation of immiscible liquids, crystallization differentiation of magmatic melts, and their interaction with mantle material [1]. One of the most convincing arguments for the magmatic genesis of carbonatites was provided by J. Dawson, who observed carbonatite lava eruptions from Oldoninyo Lengai volcano. Genetically related magmatic pyroxenites, ijolites, and nepheline syenites of intrusive facies occur as fragments in the pyroclastic deposits of this volcano [2]. When the intrusive facies of alkaline–ultramafic complex are studied, the researchers inevitably face the problem of the dualistic (magmatic and metasomatic) nature of these rocks.

Alkaline–ultramafic massifs with carbonatites are known in the central Cis-Sayan area (Belaya Zima Complex) and southeastern Cis-Sayan (Zadoi) areas (Fig. 1). The Zadoi (Zhidoi) Massif differs from the Belaya Zima group of massifs in more weakly pronounced metasomatic processes. Some of its rocks show no traces of secondary alterations. Based on the petrographic and mineralogical studying of the rocks, a hypothesis was advanced that the apatite- and perovskite bearing clinopyroxenites crystallized from magmatic melts, and the mineralized (perovskite and ilmenite) clinopyroxenite, ijolites, and nepheline syenites are comagmatic [3, 4]. Carbonatites in the central and southeastern parts of the Cis-Sayan ledge are characterized by a depleted composition in Nd and Sr diagrams [5]. The scatter of the Rb–Sr and Sm–Nd isotopic systems of the carbonatites was interpreted as a consequence of the mixture of two mantle components [6]. Our trace-element data and recently determined Sr isotopic compositions of the rocks enabled us to analyze the geochemical evolution of magmatism in the Zadoi Massif within the framework of the concept of the successive involvement and melting of material from various sources.

GEOLOGY AND PETROGRAPHY OF THE MASSIF

The Zadoi Massif in the Early Precambrian Sharyzhalgai block of the Cis-Sayan basement ledge of the Siberian Platform is hosted in alternating pale gray biotite, biotite–hornblende, hypersthene, and two-

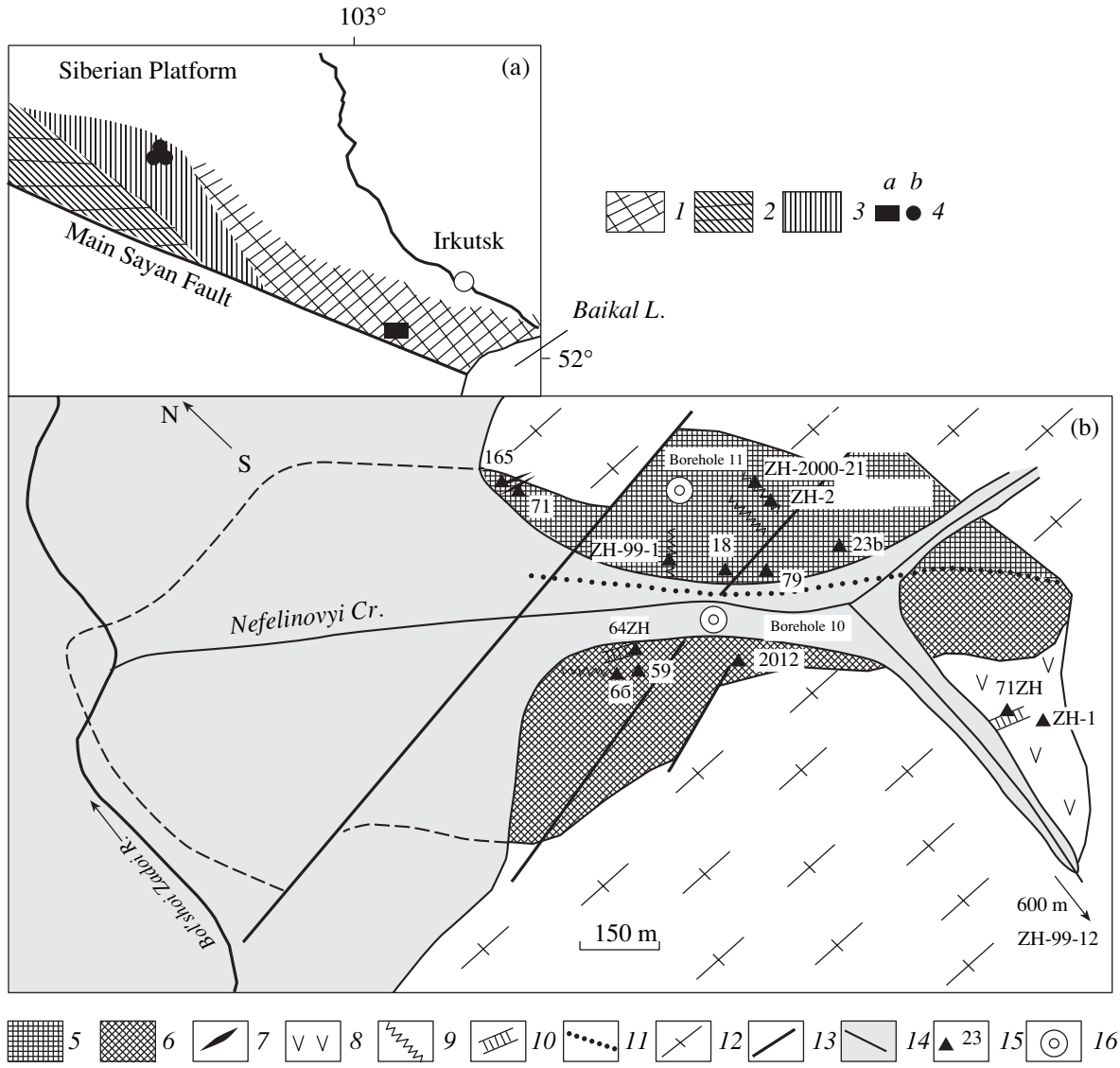

Fig. 1. (a) Location map and (b) sampling map of the Zadoi alkaline–ultramafic massif (modified after schematic maps in [3]). (*1–3*) Cis-Sayan basement ledge of the Siberian Platform: (*1*) Sharyzhalgai block, (*2*) Biryusa block, (*3*) Urik–Iya graben; (*4*) Zadoi Massif (a) and massifs of the Belaya Zima Complex (b); (*5*) Ilmenite clinopyroxenites; (*6*) perovskite clinopyroxenites; (*7*) afrikandite and apatite–titanomagnetite clinopyroxenite veins cutting ilmenite clinopyroxenites; (*8*) ijolite–melteigite rocks; (*9*) nepheline syenite dikes; (*10*) carbonatite veins; (*11*) boundary between the facies of perovskite and ilmenite clinopyroxenites of the first phase; (*12*) biotite and two-pyroxene plagioclase schists and gneisses of the Early Precambrian basement; (*13*) inferred faults; (*14*) modern alluvium and inferred contour of the northwestern part of the massif beneath it; (*15*) sample numbers; (*16*) boreholes: Borehole 10 (samples 0, 1, 2, 18, 26, 31, 37, 39, 51, 58, 68, 74, and 94), Borehole 11 (sample 83).

pyroxene gneisses and dark gray crystalline plagioclase schists.

The massif comprises four evolutionary phases [3, 4]: (i) a phase of the emplacement of a large magmatic body of mineralized clinopyroxenites; (ii) a crystallization phase of ijolites and ijolite-like rocks; (iii) a phase of the emplacement of nepheline syenite dikes; and (iv) a phase of the origin of carbonatite veins. According to borehole drilling materials, the ilmenite clinopyroxenites dip beneath the perovskite clinopyroxenites. In vertical Borehole 10, the perovskite clinopyroxenites compose the uppermost 100 m and are underlain by ilmenite clinopyroxenites. The contact between the bodies of ilmenite and perovskite mineralized clinopyroxenites trends to the northwest. The ilmenite clinopyroxenites near the contact bear veins of afrikandites and apatite–titanomagnetite clinopyroxenites (Fig. 1, samples 165 and 71, respectively).

The perovskite clinopyroxenites are medium-grained black rocks with a trachytoid texture, which consist of clinopyroxene (up to 70%), titanomagnetite (15%), apatite (7%), perovskite (6.5%), ilmenite (1%), and accessory brown hornblende, biotite, titanite, pyrrhotite, pentlandite, chalcopyrite, and pyrite. The afrikan-

dites are fine-grained black massive rocks consisting of perovskite (33%), pyroxene (25%), apatite (up to 14%), amphibole, ilmenite, and interstitial titanomagnetite (22%). Small monomineralic veins were found that consisted of perovskite or titanomagnetite.

The ilmenite clinopyroxenites differ from the perovskite clinopyroxenites in having a dark gray color and finer grained textures. Compared with the perovskite clinopyroxenites, they contain more clinopyroxene (up to 76%) and ilmenite (7.5%) but less titanomagnetite (10%) and apatite (6%). The accessory minerals are sulfides and, occasionally, perovskite.

According to their composition, geological setting, and genesis, the rocks of the second phase are classified into magmatic rocks (micrograined feldspar ijolites in thin dikes and medium-grained melteigites in a thicker dike) and metasomatic rocks (ijolites–melteigites in the southeastern margin of the massif, which were formed during the nephelinization of the mineralized pyroxenites).

Dikes and veins of the third-phase syenites cut the body of the mineralized clinopyroxenites and partly extend beyond it. Within the facies of the perovskite clinopyroxenites of the first phase, nepheline syenite veins consist of coarse-grained and pegmatoid rocks, whereas these veins in the ilmenite pyroxenite facies and wall rocks are fine-grained. The nepheline syenites consist of nepheline (16.4%), anorthoclase (53.4%), cancrinite (15.7%), aegirine-augite (11.7%), and biotite (2%), with accessory amounts of zircon, titanite, clinozoisite, and calcite.

Carbonatite veins of the fourth phase were emplaced into the perovskite pyroxenites and metasomatic melteigites. These are coarse-grained yellowish white massive rocks, which are quantitatively dominated by calcite with minor amounts of biotite, apatite, and sulfides. The carbonatites contain accessory pyrochlore.

AGE

The Zadoi Massif was dated by several researchers. Two samples of its nepheline syenites yielded whole-rock K–Ar ages of 644 and 596 Ma, and their anorthoclase, nepheline, and cancrinite were dated at 632–415 Ma [7]. The measured ratios of radiogenic Ar and K of coarse-tabular vermiculitized biotite from pockets in the outer contact zone of a carbonatite vein yielded an age of 625 ± 18 Ma [8]. The results of the Rb–Sr and Sm–Nd geochronometric studies of the Zadoi Massif were published in [6]. The slope of regression lines drawn through the data points of the ijolite, nepheline syenite, and one point of the carbonatite in a Rb–Sr isochron diagram yielded an approximate age of the massif equal to 569 ± 42 Ma at $(^{87}Sr/^{86}Sr)_0$ 0.703403 ± 0.000106. In a Sm–Nd diagram, the data points are widely scattered, and the regression equation yielded an age of 612 Ma with an error of ±677 Ma, which was greater than the age value itself. Similarly to the K–Ar dates, these data are generally consistent with the previously assumed Late Precambrian geological age of alkaline–ultramafic complexes in the area. The K–Ar dates were distorted because of the presence of excess Ar, and no whole-rock Rb–Sr and Sm–Nd isochrons were obtained because both of the isotopic systems occurred to be heterogeneous due to the arrival of the magmatic melts from deep sources with various isotopic characteristics. The massif was dated by the $^{40}Ar/^{39}Ar$ method with stepwise heating of the feldspar–nepheline mixture separated from nepheline syenite (sample ZH-99-12). The plateau age of the nepheline is 547.8 ± 6.6 Ma [9].

The previously published K–Ar and Rb–Sr ages of metasomatically altered rocks of alkaline–ultramafic complexes in the Cis-Sayan area broadly vary, from the Late Precambrian to Early Paleozoic (700–500 Ma) [7, 10, and others]. The Rb–Sr dating of an unaltered nepheline dike yielded an $^{40}Ar/^{39}Ar$ age close to the age of the Zadoi Massif. Clinopyroxene, biotite, and nepheline from the groundmass and phenocrysts were dated at 547.0 ± 8.3 Ma (±2σ) at $(^{87}Sr/^{86}Sr)_0 = 0.70308 \pm 0.00019$ (MSWD = 3.17), and biotite and two nepheline fractions gave an age of 546.1 ± 2.2 Ma (±2σ) at $(^{87}Sr/^{86}Sr)_0 = 0.70359 \pm 0.00074$ (MSWD = 0.93) [11].

The $^{40}Ar/^{39}Ar$ and Rb/Sr dates of unaltered rocks of alkaline–ultramafic complexes in the central and southeast parts of the Cis-Sayan uplift coincide (within the analytical errors) with the age of the Precambrian–Cambrian boundary (542 Ma), which was determined in a reference stratigraphic section in Oman [12].

MAJOR OXIDES

The mineralized clinopyroxenites of the first phase bear no more than 1.6 wt % alkalis at moderate contents of MgO (8–11.6 wt %) and high concentrations of CaO (16–21 wt %) and TiO_2 (5–12 wt %). Magmatic veins of the second-phase ijolites and melteigites of the massif are chemically similar to volcanic melilitites. The vein nepheline syenites of the third phase are highly alkaline (15–16 wt % of the sum of alkalis) and are comparable with foidlites. The carbonatites belong to the calcic type and contain 54–56 wt % CaO and 39–42 wt % CO_2 (Table 1).

The perovskite clinopyroxenites contain more TiO_2 and less (FeO + Fe_2O_3) as the MgO concentrations increase. The maximum TiO_2 concentration (11.6 wt %) was determined in the most magnesian perovskite clinopyroxenite (sample 0). The less magnesian perovskite clinopyroxenites bear less TiO_2 (10.4 wt %). The most magnesian ilmenite clinopyroxenite (sample 74) containing 6.6 wt % TiO_2 and the samples 83 and 18 belong to the group of low-Ti magmatic ilmenite clinopyroxenites. The MgO contents in this rock group decreases with increasing TiO_2 contents. The low magnesian part of the trend defined by the ilmenite clinopyroxenite passes through the data points of rocks enriched in P

Table 1. Major- (wt %) and trace-element (ppm) composition of representative rock sample from the Zadoi Massif

Component	1	2	3	4	5	6	7	8	9	10	11	12	13	14	15	16
	0	1	31	2012	74	83	18	79	58	51	39	71	Zh-99-12	Zh-1	23-b	64-zh
SiO_2, wt %	29.60	29.78	27.22	24.98	33.14	34.93	33.24	32.07	37.35	32.68	32.92	18.13	51.45	44.86	0.08	0.36
TiO_2	11.58	11.05	10.44	11.00	6.56	5.57	5.68	9.27	7.79	9.11	5.06	8.23	0.45	1.43	0.02	<d.l.
$A1_2O_3$	5.50	5.30	4.20	6.08	5.30	4.70	4.70	5.50	7.20	5.30	4.40	4.20	19.65	19.70	<d.l.	0.03
Fe_2O_3	9.13	8.06	18.11	15.48	12.80	11.19	11.14	10.85	5.43	10.49	10.17	16.69	3.95	4.20	n.a.	1.54
FeO	8.74	8.40	11.15	7.60	8.30	8.35	9.67	9.20	13.14	10.59	10.40	14.76	1.76	2.25	0.50	1.00
MnO	0.16	0.16	0.39	0.12	0.24	0.20	0.19	0.23	0.29	0.33	0.27	0.28	0.19	0.37	0.31	0.21
MgO	11.90	10.51	5.88	9.58	11.46	10.89	10.09	10.47	8.64	7.21	9.25	7.88	0.46	0.67	0.15	0.40
CaO	19.04	21.28	17.92	22.22	8.90	19.88	19.88	18.48	15.96	19.32	20.44	18.76	3.34	8.12	56.04	54.38
Na_2O	0.33	0.43	0.61	0.46	0.51	0.61	0.55	0.40	1.30	0.68	0.76	0.40	9.14	6.39	0.12	0.09
K_2O	0.07	0.10	0.08	0.00	0.16	0.18	0.32	0.16	0.27	0.09	0.61	0.18	6.82	3.82	<d.l.	no
P_2O_5	2.73	3.55	2.42	1.37	1.88	2.39	3.00	2.19	1.26	1.70	3.48	8.84	0.10	0.28	<d.l.	0.19
H_2O^-	0.12	0.03	0.08	n.a.	0.30	0.08	0.02	0.02	0.02	0.02	0.05	0.03	0.17	0.43	n.a.	n.a.
H_2O^+	n.a.	n.a.	n.a.	0.84	n.a.	n.a.	n.a.	n.a.	1.08	1.91	2.08	1.42	2.83	3.67	n.a.	n.a.
CO_2	n.a.	n.a.	n.a.	n.a.	n.a.	n.a.	n.a.	n.a.	n.a.	n.a.	n.a.	n.a.	n.a.	0.66	42.35	41.25
Total	98.90	98.65	98.50	98.89	99.55	98.97	98.48	98.84	99.73	99.43	99.89	99.80	100.31	96.85	99.63	99.93
Sc, ppm	48.8	60.1	18.8	40.2	65.4	70.3	47.6	53.6	50.0	46.0	19.2	38.9	3.78	4.12	4.12	0.94
Rb	1.53	3.63	2.24	2.61	3.69	5.09*	7.67*	5.38	4.39	20.1*	1.62	5.72*	118	81.6	9.10	7.83
Sr	759	732	972	772	384	504*	594*	594	1098	898*	858	866*	1771	2493	16622	15266
Y	87.6	76.2	125	72.6	23.8	25.1	30.3	51.4	47.7	44.9	107	56.2	14.0	134	254	227
Zr	534	385	1555	480	343	257	280	462	270	302	1546	210	598	1733	n.a.	n.a.
Nb	318	233	468	311	10.4	17.2	15.3	127	117	22.1	403	18.1	150	245	1.65	53.9
Cs	0.03	0.03	0.03	0.27	0.05	0.08	0.09	0.05	0.24	0.61	0.09	0.10	1.13	2.25	n.a.	n.a.
Ba	57.9	55.5	22.3	286	42.0	66.5	119	106	320	147	10.9	65.1	1573	1249	933	1238

Table 1. (Contd.)

Component	1	2	3	4	5	6	7	8	9	10	11	12	13	14	15	16
	0	1	31	2012	74	83	18	79	58	51	39	71	Zh-99-12	Zh-1	23-b	64-zh
La	413	622	287	370	48.8	54.0	66.8	342	99.5	116	201	159	46.6	198	977	928
Ce	857	1803	612	111	132	140	222	987	305	256	431	370	99.5	442	1749	1660
Pr	108	261	72.0	89	22.2	22.1	27.1	110	33.4	33.4	49.9	47.6	9.92	32.8	213	200
Nd	468	1015	262	364	98.8	94.1	120	471	136	169	193	248	32.6	119	723	652
Sm	70.9	113	46.1	59.2	16.7	16.4	20.2	62.3	22.5	28.2	35.4	42.2	4.97	22.5	75.7	63.2
Eu	18.5	25.7	13.3	17.0	4.50	4.34	5.42	14.7	5.00	6.98	11.0	10.7	1.53	6.24	18.5	15.3
Gd	54.2	72.2	45.1	53.0	13.6	13.3	16.1	43.1	18.3	22.3	33.4	32.7	3.74	18.2	52.3	44.3
Tb	6.42	7.21	5.50	5.94	1.52	1.49	1.80	4.43	2.20	2.60	4.61	3.59	0.51	2.59	8.83	7.46
Dy	26.0	27.9	26.7	24.3	6.57	6.50	7.78	17.6	10.5	10.7	23.1	14.1	3.02	20.1	30.3	25.1
Ho	3.85	3.49	4.51	3.75	0.95	0.95	1.13	2.34	1.78	1.67	3.86	2.11	0.54	3.39	5.46	4.62
Er	7.32	6.44	10.2	7.44	1.96	2.15	2.42	4.61	4.20	3.43	8.93	3.99	1.47	10.5	17.1	14.8
Yb	3.81	2.97	6.15	3.99	1.35	1.38	1.54	2.49	3.19	2.22	5.79	2.23	1.38	8.46	11.0	9.66
Lu	0.45	0.36	0.83	0.48	0.21	0.21	0.20	0.34	0.46	0.31	0.72	0.27	0.31	1.21	1.62	1.39
Hf	20.2	14.2	46.1	19.6	14.6	10.8	10.0	18.7	9.91	10.0	48.0	7.60	13.9	31.4	n.a.	n.a.
Ta	31.2	35.6	34.0	29.9	1.34	1.44	1.25	22.8	7.78	1.26	29.3	1.53	2.40	3.69	0.13	0.43
Pb	3.84	2.53	0.54	n.a.	3.38	0.31	0.40	3.41	2.10	1.97	0.63	0.84	6.38	15.9	10.1	13.9
Th	33.2	129	5.06	24.3	1.82	3.13	2.30	50.9	3.87	4.47	3.12	4.84	6.13	26.0	1.46	1.49
U	8.31	6.05	1.24	9.13	0.35	0.57	0.41	3.90	0.54	0.85	1.03	0.75	2.31	10.3	0.07	5.45

Notes: (1–10) Mineralized pyroxenites: (1–4) perovskite pyroxenites, (5–10) ilmenite pyroxenites; (11–12) veins in ilmenite clinopyroxenites of (11) titanite and (12) apatite–titanomagnetite clinopyroxenites; (13) nepheline syenite; (14) ijolite; (15–16) carbonatites. Detection limits (d.l.): Al_2O_3–0.25, K_2O–0.01, P_2O_5–0.03 wt %; n.a. means not analyzed. Major oxides were analyzed by conventional analytical techniques at the Analytical Center of the Institute of the Earth's Crust, Siberian Division, Russian Academy of Sciences (analysts G.V. Bondareva and M.A. Smagunova). Trace elements were determined by ICP-MS with the preliminary preparation of the samples at the Laboratory of Isotopic Research and Geochronology of the Institute of the Earth's Crust, Siberian Division, Russian Academy of Sciences, with the microwave decomposition (analyst M.E. Markova). The chemical decomposition of the carbonatite was started with the treatment of the sample with concentrated HNO_3. The measurements were conducted at the Irkutsk Analytical Center for Collective Use on a VG Plasmoquad PQ2+ mass spectrometer.

* Measurements by the isotopic dilution techniques. Analyses 4 and 16 present data on major oxides from [3].

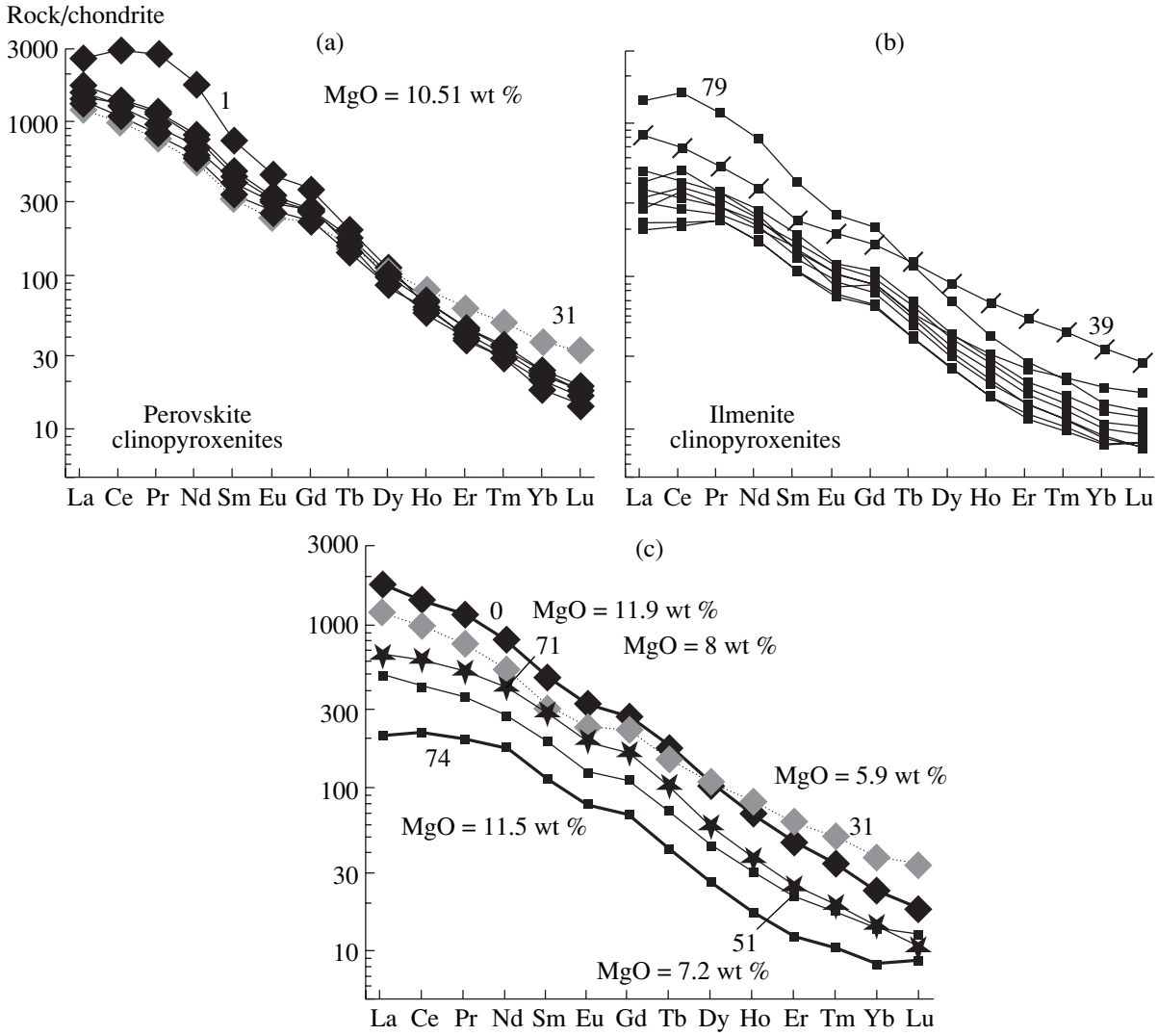

Fig. 2. Chondrite-normalized REE patterns of (a) perovskite and (b) ilmenite clinopyroxenites and (c) varieties of these rocks with the maximum and minimum MgO concentrations. Chondrite composition is according to [13].

and Fe (apatite–titanomagnetite clinopyroxenite, sample 71) and Ti (sample 51). Titanite clinopyroxenite (sample 39) is characterized by low concentrations of TiO_2 (5 wt %). The highest contents of TiO_2 (28.6 wt %) were detected in the afrikandite (sample 165) [3].

The SiO_2 concentrations of the perovskite clinopyroxenite are no higher than 30.5 wt % at a minimum in the afrikandite (10.6 wt %) and variable concentrations in the ilmenite clinopyroxenites (from 31.8 to 37.3 wt %, Table 1). An exception is sample 68 of ilmenite clinopyroxenite, which contains 28 wt % SiO_2.

RARE-EARTH ELEMENTS

The occurrence of perovskite in the clinopyroxenites is reflected in their enrichment in REE compared to the ilmenite clinopyroxenites. The maximum concentrations of LREE were detected in sample 1, and the highest contents of HREE were found in sample 31. Samples 39 (titanite clinopyroxenite) and 79 (ilmenite clinopyroxenite) show elevated REE concentrations and intersecting REE patterns (Table 1, Figs. 2a, 2b).

The magnesian perovskite clinopyroxenites (samples 0 and 1) are characterized by low concentrations of HREE as compared to those in the low-Mg perovskite clinopyroxenite (sample 31, Figs. 2a, 2c). LREE show the opposite tendencies. In contrast to the intersecting REE patterns of the perovskite clinopyroxenites with various Mg# values, the ilmenite clinopyroxenites are characterized by subparallel REE patterns. The most magnesian ilmenite clinopyroxenite (sample 74) has low REE concentrations, and the least magnesian rock (sample 51) bears elevated REE concentrations. The apatite–titanomagnetite clinopyroxenite (sample 71) shows an intermediate Mg# value and REE concentrations (Fig. 2c).

Compared with the first-phase mineralized clinopyroxenites, the REE patterns of the second-phase ijolite displays a tendency toward a relative enrichment in HREE. The analogous tendency in the first-phase rocks is pronounced in the clinopyroxenite of sample 31 and the ilmenite clinopyroxenite of sample 39 (Figs. 2a, 2b). The third-phase nepheline syenite contains much less REE, whose concentrations increase again in the fourth-phase carbonatites, with the subparallel shift of the REE patterns relative to those of the nepheline syenites (the diagram is not shown).

INCOMPATIBLE ELEMENTS

For comparison, diagrams of the concentrations of incompatible elements in the Zadoi massif normalized to those in the undifferentiated mantle also show the patterns of basalts from oceanic islands (OIB) (Fig. 3). The mineralized clinopyroxenites bear concentrations of the most incompatible elements (Cs, Rb, Ba, and K) similar to or lower than those of OIB. The concentrations of Th–U, Nb–Ta, and the following elements are higher than in OIB. This drastic shift of the concentrations testifies to the depletion of the mantle source of the mineralized clinopyroxenites in the most incompatible elements.

Both the perovskite and ilmenite clinopyroxenite show clearly pronounced Pb and Sr minima (Figs. 3a, 3b). Because of their low Pb concentrations, both groups of the mineralized clinopyroxenites have very high Ce/Pb ratios (up to 3000), much higher than in oceanic basalts (25 ± 5). Similarly, the low Sr concentrations in both groups of the mineralized pyroxenites results in their high Pr/Sr ratios (up to 0.4), which are also much higher than in oceanic basalts, including OIB (0.015, Fig. 4). The mineralized clinopyroxenites differ from OIB in having low K/Nb, Nb/Ta, and Sr/Nd ratios.

In the main group of the perovskite clinopyroxenites, the concentrations of incompatible elements vary insignificantly. The maximally contrasting distribution of these elements was detected in one of the magnesian samples (sample 1 with the maximum concentrations of Th and LREE) and in the least magnesian one (sample 31 with the minimum concentrations of Th, U, Pb, and the maximum contents of Nb, Zr, Hf, Y, and Yb).

The main group of the ilmenite clinopyroxenites show deep Pb minima. Anomalous concentrations with the tendency of the perovskite clinopyroxenite were detected in the low magnesian sample 39 (low Rb, Ba, high Nb, Ta, Zr, Hf, Y, and Yb) and high-Ti sample 79 (high Th, U, Nb, Ta, and REE). Two low-Mg samples differ from the main group of the ilmenite clinopyroxenites in having elevated concentrations of the most incompatible elements: Cs, Rb, Ba, and Th (sample 51) and Cs, Ba (sample 58). The latter sample also has elevated concentrations of Nb, Ta. The apatite–titanomagnetite clinopyroxenite of sample 71 bears concentrations of incompatible elements comparable with those in the main group of the ilmenite clinopyroxenites.

Incompatible elements in the second-phase ijolite differ from elements in the mineralized clinopyroxenite by the absence of depletion in the most incompatible elements and by a smoother pattern, which is close to those of OIB. The pattern of the normalized concentrations of most elements passes above the pattern of OIB and nearly parallel to it, having small minima at Ba, Rb, K, Ta, P, and Ti.

The nepheline syenites of the third phase have concentrations of incompatible elements close to those in the ijolite of the second phase in the left-hand part of the succession, from Cs to Ta (with the minimum shifted to Th, U), and this pattern descends below the ijolite pattern in the right-hand part, starting at La (Fig. 3c). The nepheline syenites have Ba/La, Nb/La, Zr/Sm, Zr/Hf, Sr/Nd, and Nb/Ta ratios higher than those in OIB but Ce/Pb and Pr/Sr ratios lower than in OIB.

Incompatible elements in the fourth-phase carbonatites is subdivided into two groups. One of them includes elements from Rb to Ta, and the other comprises elements from La to Yb (Fig. 3c).

The first-group elements plot below the nepheline syenites (except a Ba maximum), while the elements of the second group are above it. The transition from left to right in the carbonatites, from the group of relatively low normalized concentrations of incompatible elements to the group with higher concentrations, coincides with the opposite transition of incompatible elements in the nepheline syenites in the left-hand part to the group of lower concentrations in the right-hand part. These are complementary relations between the sources of the nepheline syenites and carbonatites.

INITIAL SR ISOTOPIC RATIOS

The Sr concentrations in the mineralized clinopyroxenite are two orders of magnitude higher than the Rb concentrations. Recalculations to the age of massif of 548 Ma yield initial ratios that differ from the measured ones by 0.0003 on average. The values of 10000/Sr and $(^{87}Sr/^{86}Sr)_0$ of the perovskite clinopyroxenites vary within narrow ranges, from 10 to 14 and from 0.702469 to 0.70285, respectively. The maximum Sr isotopic ratio of this group was detected in apatite from sample 6b. Close initial Sr isotopic ratios in the apatite, pyroxene, and perovskite (Table 2) testify to the concurrent crystallization of these minerals. The perovskite clinopyroxenites are denoted by PC in Fig. 5b.

The Sr concentrations in the ilmenite clinopyroxenite vary within broader range at $(^{87}Sr/^{86}Sr)_0 = 0.7030–0.7036$. The lower-limit points of this range are close to the values of the perovskite clinopyroxenites (composition PC), and the upper-limit points plot not far from the points of the ijolites and nepheline syenites (composition A). Some of the ilmenite clinopyroxenites with elevated 10000/Sr values are denoted by composition IC.

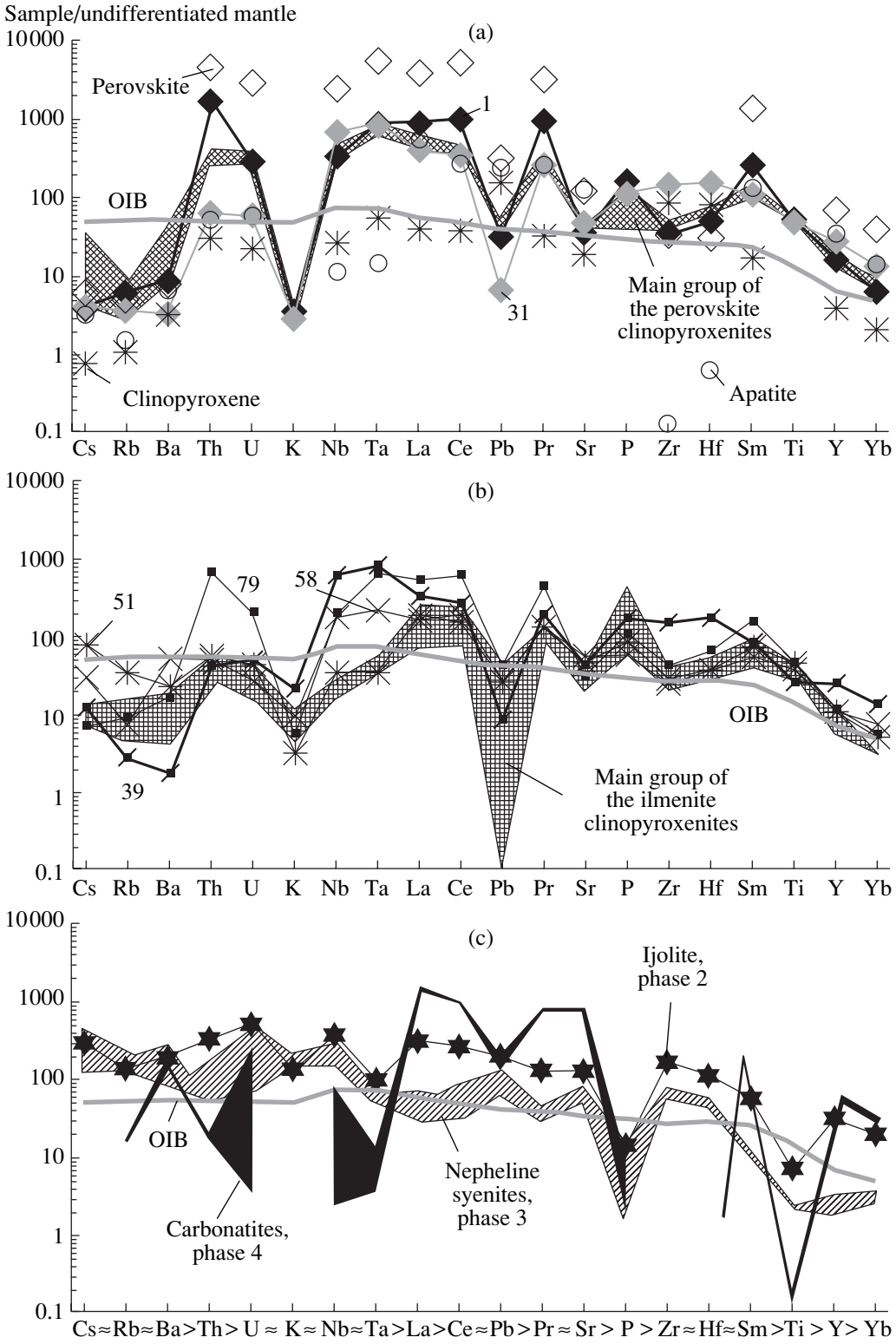

Fig. 3. Incompatible-element patterns normalized to the undifferentiated mantle for the mineralized clinopyroxenites of the first phase (a—perovskite, b—ilmenite) and (c) rocks of the later three phases of the Zadoi Massif. The diagram (a) also shows the compositions of rock-forming minerals from sample 6-b (without K, P, and Ti). The compositions of OIB and the undifferentiated mantle are according to [13]. Symbols ≈ and > at the abscissa indicate relations of incompatible elements in oceanic basalts. In normalizing Cs and Pb, we used coefficients equal to 0.0079 and 0.079, respectively.

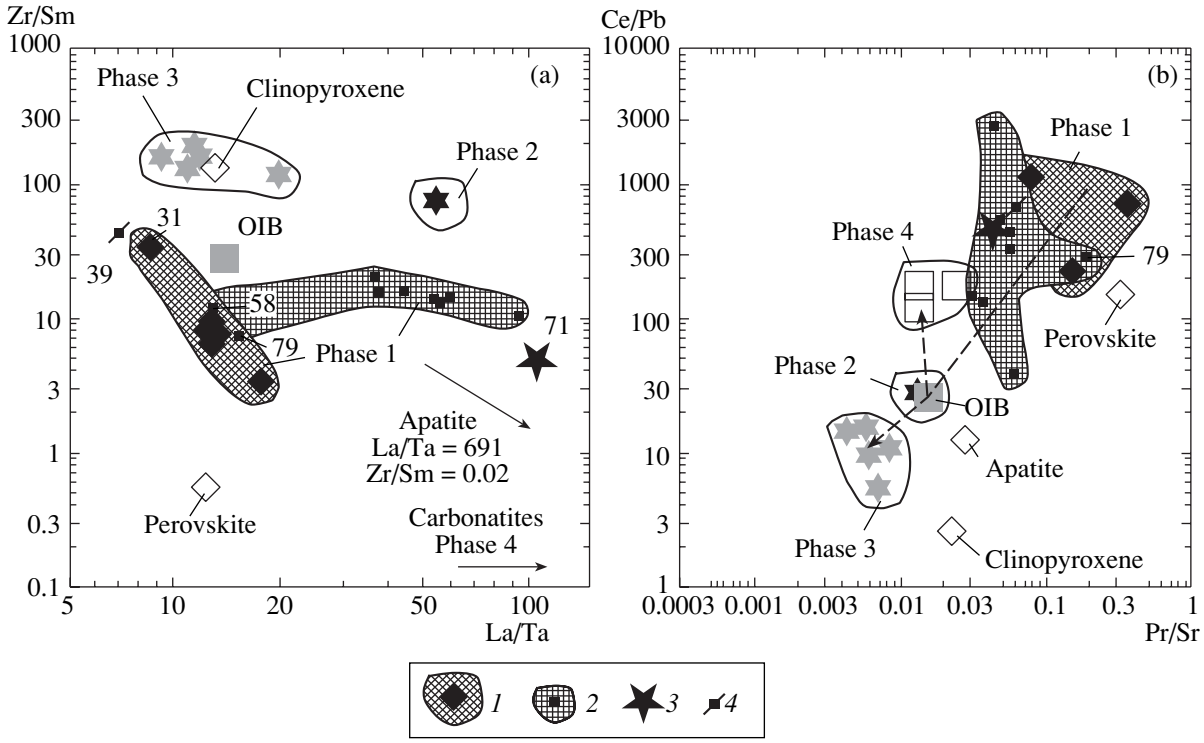

Fig. 4. (a) Zr/Sm vs. La/Ta and (b) Ce/Pb vs. Pr/Sr diagrams for the rocks of four phases of the Zadoi Massif and the rock-forming minerals of the perovskite clinopyroxenites. The generalized magmatic evolution is shown as a dashed line with branching arrows in Fig. (b). (*1*) Group of perovskite clinopyroxenites; (*2*) group of ilmenite clinopyroxenites; (*3*, *4*) veins in ilmenite clinopyroxenites: (*3*) apatite–titanomagnetite clinopyroxenites (sample 71), (*4*) titanite clinopyroxenites (sample 39).

The apatite–titanomagnetite clinopyroxenite of sample 71 has an intermediate $(^{87}Sr/^{86}Sr)_0$ value of 0.702918 and plots in Fig. 5b onto the line connecting compositions PC and A.

Similar $(^{87}Sr/^{86}Sr)_0$ values of 0.704144 and 0.703462 values were determined for the ijolite and nepheline syenite, respectively, at overlapping ranges of Sr concentrations (1240–2493 and 1013–1771 ppm). The variations in the 10000/Sr values in these rocks within the range from composition A1 to A2 reflect the processes of element fractionation in the isotopically homogeneous source of A (Fig. 5b).

The Sr concentrations of the carbonatites are three orders of magnitude higher than their Rb concentrations, and hence, the measured Sr isotopic ratios of these rocks correspond to their initial ratios (Table 2). The Sr isotopic ratio of the carbonatites increases from 0.7029 to 0.7034 with increasing 10000/Sr (a decrease in the Sr concentration from 16622 ppm in sample 23-b to 4660 ppm in sample TA-5). The maximum ratio of 0.70403 was measured in carbonatite 71-zh, which shows geochemical evidence of secondary alterations and contamination with the material of the Archean crust (elevated K concentrations that are atypical of carbonatites). The data points of the unaltered carbonatites define a mixing trend between two end members in Fig. 5a. One of these end members, component C(A), is carbonatite material comparable with the source of A in terms of Sr isotopic ratio. The other, component C (PC, IC), is regarded as material derived from the sources of the ilmenite and perovskite clinopyroxenites (Fig. 5b).

DISCUSSION

The local character of alkaline–ultramafic magmatism with carbonatites in the Zadoi Massif and the relations between the rocks of its four phases suggest that the massif was formed by a common magmatic process within a limited time span. Judging from the fact that afrikandite veins intersect the ilmenite clinopyroxenites of the first phase, the perovskite-bearing melts crystallized after the ilmenite-bearing ones. At the same time, the nepheline syenite melts produced vein pegmatoid and coarse-grained rocks owing to their relative thermal isolation in the still-hot body of the perovskite clinopyroxenites but were quickly quenched due to heat sink into the wall rocks and the earlier ilmenite clinopyroxenites.

The systematic trends in the elemental ratios (Fig. 4) and the evolution of the Sr isotopic composition in the succession of the unaltered magmatic rocks of the Zadoi Massif were directed from perovskite and ilmenite clinopyroxenites (PC and IC) to the ijolites and nepheline syenites (compositions of source A) and further to carbonatites [C(A)–C(PC, IC) compositions] (Fig. 5). In this succession, the key role was played by

Table 2. Mass spectrometric measurements of Rb and Sr concentrations and isotopic ratios in rocks and minerals from the Zadoi Massif

Sample no.	Rock, mineral	Rb	Sr	$^{87}Sr/^{86}Sr$	$\pm\sigma$, 10^{-6}	$(^{87}Sr/^{86}Sr)_0$
18	Ilmenite clinopyroxenite	7.67	594	0.703528	13	0.703233
51	Ilmenite clinopyroxenite	20.1	898	0.704076	20	0.703566
83	Ilmenite clinopyroxenite	5.09	504	0.703383	13	0.703152
68	Ilmenite clinopyroxenite	9.24	566	0.703350	12	0.702977
71	Apatite–titanomagnetite clinopyroxenite	5.72	866	0.703069	20	0.702918
TA-1	Perovskite clinopyroxenite	0.67	768	0.702489	14	0.702469
6b-pvs	Perovskite	2.72	2399	0.702825	18	0.702799
6b-ap	Apatite	0.90	2613	0.702860	13	0.702852
6b-px	Clinopyroxene	0.63	399	0.702850	12	0.702814
TA-3	Ijolite	33.60	1240	0.704144	11	0.704144
TA-4	Nepheline syenite	105	882	0.706185	12	0.703462
71-zh	Carbonatite	6.01	7120	0.704070	9	0.704070
64-zh	Carbonatite	7.83	15266	0.702963	12	0.702963
23-b	Carbonatite	9.10	16622	0.702865	12	0.702865
TA-5	Carbonatite	1.79	4660	0.703389	11	0.703389
TA-6	Carbonatite	1.03	6050	0.703351	6	0.703351
Zi 327	Carbonatite	2.65	7770	0.703182	14	0.703182
Zi 316/3	Carbonatite	0.48	13600	0.703004	14	0.703004

Note: Sr isotopes were analyzed at the Laboratory of Isotopic Research and Geochronology of the Institute of the Earth's Crust, Siberian Division, Russian Academy of Sciences. Samples were decomposed in air in Teflon vessels, using mixtures of concentrated HF and HNO_3. Sr was extracted on chromatographic columns with an inner diameter of 8 mm, filled with 5 cm^3 of Dowex 50 × 80 anion exchanger (200–400 mesh). The eluant was 2 N HCl . Sr isotopic ratios and concentrations in samples with tracers were determined in the course of a single analysis on a Finnigan MAT 262 mass spectrometer at the Irkutsk Analytical Center for Collective Use. During the measurements, the average values of the Sr isotopic standard NBS SRM 987 were 0.71028 ± 0.00002. When Rb concentrations were measured by the isotopic dilution technique, the $^{87}Rb/^{85}Rb$ ratio in samples with tracers were measured on a MI-1201 TM mass spectrometer at the Laboratory of Isotopic Research and Geochronology of the Institute of the Earth's Crust. Data on samples TA-1, TA-4, TA-5, TA-6, Zi 327, Zi 316/3, and TA-3 were compiled from [6].

the transitions (i) from the perovskite and ilmenite pyroxenites to ijolites and nepheline syenites and (ii) from the ijolites and nepheline syenites to carbonatites.

Sources of the Ilmenite and Perovskite Clinopyroxenites

The increase in the $(^{87}Sr/^{86}Sr)_0$ ratios from the perovskite clinopyroxenites to ijolites and nepheline syenites can be interpreted as resultant from the mixing of material with the isotopic signatures of PC (source of the perovskite clinopyroxenites) and A (source of the ijolites and nepheline syenites). An intermediate Sr isotopic composition should then reflect the result of this mixing and be expressed as the arrangement of the data points along a straight line (or lines) between compositions PC and A (within the range A1–A2). The data point of the low-Mg ilmenite clinopyroxenite of sample 51 lies within the compositional field A1–A2 and, together with the points of the perovskite and apatite–titanomagnetite clinopyroxenites, plots on the PC–A2 mixing line of Sr isotopes. The 10000/Sr values of the three data points of the ilmenite clinopyroxenites are relatively high, which suggests that at least this group of compositions was derived from a source that differed from both the source of the perovskite clinopyroxenites (PC) and the source of the ijolites–nepheline syenites (A).

The derivation of the ilmenite and perovskite clinopyroxenites from distinct sources also follows from the results of trace-element simulations conducted by the formula $C_L/C_0 = 1/[D_0 + F(1 - P)]$ [20], where C_L/C_0 is the concentration ratio of an element in the melt and melted material, F is the degree of partial melting, D_0 and P are the volumetric distribution coefficients: $D_0 = \Sigma XiDi$, $P = \Sigma MiDi$, where Xi is the proportions of minerals in the melting material, Mi is the proportions of minerals involved in melting, and Di is the mineral–melt distribution coefficient (Fig. 6).

As the melting material, we calculated the compositions of garnet peridotite with apatite, ilmenite, and perovskite: olivine (70.9%), orthopyroxene (5%), clinopyroxene (7%), garnet (7%), apatite (0.1%), and ilmenite (10%) for the ilmenite clinopyroxenites; olivine (44%),

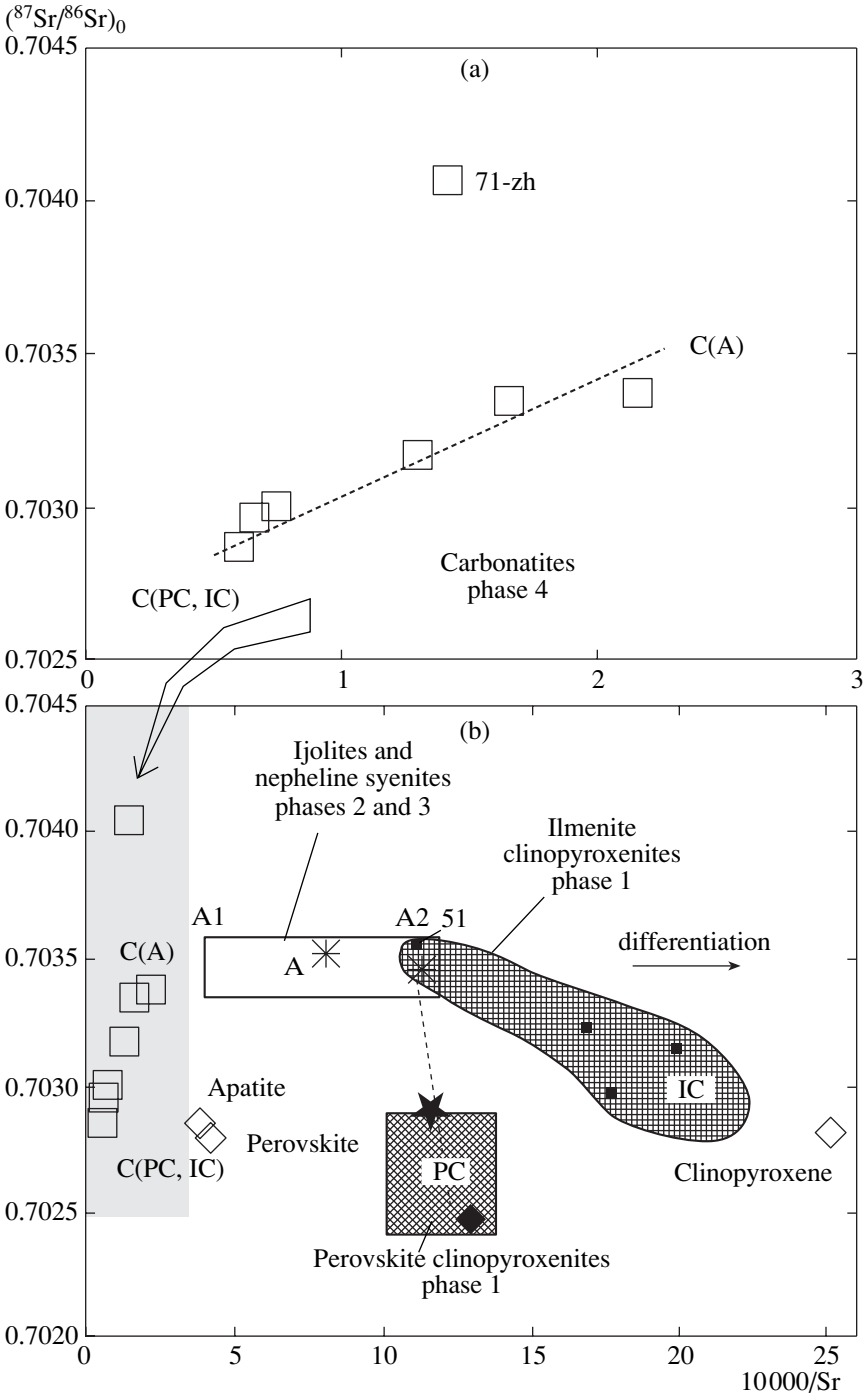

Fig. 5. Covariations in the initial Sr isotopic ratios $(^{87}Sr/^{86}Sr)_0$ and 10 000/Sr values in (a) the carbonatites of the fourth phase with a narrow abscissa range and (b) the rocks of all four phases of the massif with a broader abscissa range. Dashed lines PC–A and A1–C are mixing lines of materials with various Sr isotopic ratios (see text for explanations). Ranges of the 10 000/Sr values in the rocks of various phases are shown according to the measured Sr concentrations (Table 1). The highest $(^{87}Sr/^{86}Sr)_0$ ratios in the perovskite clinopyroxenites were assumed according to measurements in apatite from sample 6-b.

orthopyroxene (5%), clinopyroxene (5%), garnet (10%), apatite (15%), and perovskite (21%) for the perovskite clinopyroxenites. The ilmenite clinopyroxenite series was derived at 3–0.1% partial melting, whereas the perovskite clinopyroxenite series was produced at higher degrees of melting, approximately 10–20%. Some data points of the low-Mg veins of the perovskite and titanite clinopyroxenites are shifted toward compo-

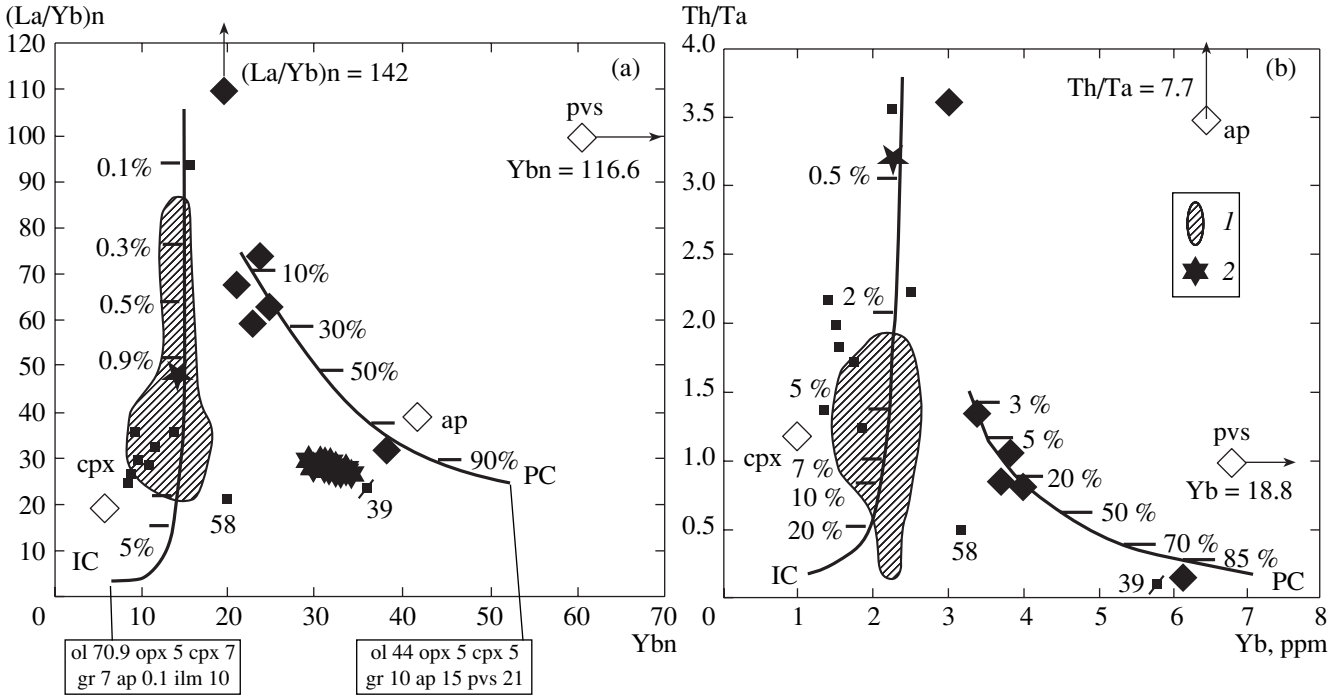

Fig. 6. (a) (La/Yb)n vs. Ybn and (b) Th/Ta vs. Yb diagrams for the simulation results obtained on the partial melting of the sources of the mineralized clinopyroxenites. See Fig. 2 for symbol explanations. (*1*) Field of olivine melilitites from South Africa [15]; (*2*) melilite–olivine nephelinites from Hamada, southwestern Japan [16]. IC and PC are the compositions of the mantle sources of the ilmenite and perovskite clinopyroxenites, respectively. Inasmuch as Ta was not determined in [16], the Hamada lavas are not shown in (b).

sitions with degrees of partial melting in the source equal to 70–80%. The perovskite contains notably elevated concentrations of Yb, and the apatite has high Th/Ta ratios. The anomalously high contents of both mineral phases in such rocks as the afrikandites can be explained by the enrichment of some melt portions in perovskite and apatite crystals during the shallow-depth crystallization differentiation.

For comparison, Fig. 6 shows the fields of high-alkali Cenozoic lavas erupted in the African continent (olivine melilitites of South Africa [15]) and the island arc of southwestern Japan (melilite–olivine nephelinites of Hamada [16]). The former characterize deep-seated alkaline magmatism in the inner part of the African plate, and the latter were erupted at approximately 6 Ma in the convergence zone of the Pacific and Eurasian plates and were derived from a source above the Pacific slab that reached depths of 500–600 km. The highly alkaline lavas of the convergence zone are compared in Fig. 6 with the perovskite clinopyroxenites of the Zadoi Massif. Their similarities are further accentuated by similarities in their patterns of incompatible elements. A distinctive feature of the melilite–olivine nephelinites of Hamada is their lower TiO_2 contents (the perovskite clinopyroxenites of the Zadoi Massif contain 10.4–11.6 wt % TiO_2, whereas the melilite–olivine nephelinites bear only ~2.6 wt % TiO_2) and less clearly pronounced relative depletion in the most incompatible elements. The comparison of the high-alkali lavas of the continental plate with the main group of the ilmenite clinopyroxenites also reveals the depleted character of the left-hand part of the elemental patterns of the Zadoi Massif. The line for the olivine melilitite closely coincides with the line for the high-Ti ilmenite clinopyroxenite of sample 79 (the comparison diagrams are not shown).

Sources of the Ijolites, Nepheline Syenites, and Carbonatites

The elevated normalized concentrations of the most incompatible elements in the left-hand part of the succession in the ijolites and nepheline syenites compared to the mineralized clinopyroxenites (Figs. 3, 4), along with the elevated initial Sr isotopic ratios, testify that the material of the second phase of the Zadoi Massif was derived from a different source. The similarities in the incompatible-element patterns of the ijolites and OIB suggest that it belonge to the sublithospheric convecting mantle.

A notable difference of the third-phase nepheline syenites from OIB is their ratios of incompatible elements. For example, while the Ce/Pb and Pr/Sr ratios of the ijolite are 28 and 13, respectively, and are close to those in OIB, both of these ratios of the nepheline syenites are much lower. The decrease in the Pr/Sr ratio

from the ijolites to nepheline syenites is associated with a relative decrease in the concentrations of Pr from 32.8 to 0.9–9.9 ppm and Sr from 2493 to 882–1771 ppm, reflecting a decrease in the concentrations of REE relative to Sr in the source of the nepheline syenites. Because of the high Sr concentrations in the ijolites and nepheline syenites, its isotopic composition could not be modified by any contamination process, and hence, should characterize the melting source material without any admixtures of materials with different Sr isotopic composition.

The carbonatites have very high Sr concentrations, and thus, the variations in its isotopic composition in these rocks reflect the analogous variations in the source (or sources). The similarities in the ranges of the Sr isotopic ratios of the carbonatites and ilmenite clinopyroxenites (Fig. 5) indicate that Sr of the carbonatite was inherited from the source (or sources) of the ilmenite clinopyroxenites. At the same time, with regard to the complementary character of incompatible-element ratios of the carbonatites and nepheline syenites (Fig. 3c), it is reasonable to suggest that the arrangement of the data points of the carbonatites in Fig. 5 was controlled by the mixing of component A of the ijolites–nepheline syenites, which was enriched in radiogenic ^{87}Sr, with a less radiogenic material. While the ilmenite and perovskite clinopyroxenites of the early phase of the massif contained a mixture of the PC–A and IC–A materials, the final-stage carbonatites show evidence of the analogous mixing of the high-Sr material A from the source of the ijolite–nepheline syenite source and the material C (PC, IC), which reflects the Sr isotopic composition of the sources of the perovskite and ilmenite clinopyroxenites.

Probable Relations between the Sources

Geological relations between the rocks of the massif suggest that the melts of the first-phase perovskite and ilmenite clinopyroxenites were emplaced roughly simultaneously, and the syenite magmas were intruded later into the still hot body of the perovskite pyroxenites. The high-Ti melts of this body could have been derived from the sublithospheric mantle or lower lithosphere. Depending on this, the deep magmatism could evolve according to two scenarios.

The high-Ti depleted material (component PC of the source of the perovskite clinopyroxenite) could ascend in the form of droplet-shaped segregations through the convecting upper mantle in the convergence zone above the deep part of the subducted slab. The degree of decompression melting in this material was approximately 10–20%. Occurring in contact with the basement of the lithosphere, which was in isotopic equilibrium with the sublithospheric convecting mantle (component A of the ijolite source), it caused metasomatism in the lithospheric material and its partial (0.1–3%) melting. The latter produced component IC of the source of the ilmenite clinopyroxenites. Later portions of the partial melts (which produced the ijolites) were dominated by the material of the sublithospheric convecting mantle (component A). Its interaction with the material of sources PC and IC and the induced onset of liquid immiscibility (or fluid differentiation) gave rise to the nepheline syenites (without shift in the Sr isotopic component, i.e., without contamination) and carbonatites, when component C(A), derived from the sublithospherc convecting mantle, mixed with the material of C (PC, IC), derived from the source of the mineralized clinopyroxenites.

The high-Ti depleted material (source PC of the perovskite clinopyroxenite) could exist as local heterogeneities in the lower lithosphere. When the convection instability of the upper mantle became more significant, these heterogeneities serve as centers of magma generation with high degrees of partial melting. The ambient mantle produced melts with lower degrees of partial melting (source IC of the ilmenite clinopyroxenites). The material of both sources mixed with the material of the sublithospheric convecting mantle (component A) and, analogously with the previous scenario, the magmatic evolution was associated with the origin of the association of nepheline syenites and carbonatites.

CONCLUSIONS

Alkaline–ultramafic massifs with carbonatites were intruded into the Cis-Sayan marginal uplift of the Siberian Platform at the Precambrian–Cambrian boundary. The timing of the magmatic events at 548 Ma was determined by the dating of unaltered nepheline syenites of the Zadoi Massif and the nepheline syenites of the Belaya Zima Complex. The evolution of the Zadoi Massif involved the emplacement of melt phases of perovskite and ilmenite clinopyroxenites, ijolites, nepheline syenites, and carbonatites. Our data on the trace-element and Sr isotopic signatures of the unaltered rocks indicate that the emplaced magmatic melts were derived from different types of mantle sources.

The source of the perovskite clinopyroxenites had incompatible-element patterns notably different from those of OIB (the material of the sublithospheric convecting mantle) and was characterized by a strongly depleted Sr isotopic composition ($(^{87}Sr/^{86}Sr)_0$ = 0.70247–0.70285). Eruptions of Cenozoic high-alkali lavas with this incompatible-element composition are known in the convergence zone of the Pacific and Eurasian plates. Anomalous characteristics of the source of the perovskite and ilmenite clinopyroxenites are its high Ce/Pb (223–1132) and Pr/Sr × 1000 (70–360) ratios. These ratios in the ilmenite clinopyroxenites significantly vary and partly approach those of OIB (decreasing to 39 and 30, respectively). Simultaneously the $(^{87}Sr/^{86}Sr)_0$ ratio increases to 0.7030–0.7036. High-alkali lavas of such incompatible-element composition are spread quite widely in the African continent. The results of trace-element simulations indicate that the perovskite clinopyroxenites could be derived at higher

degrees of partial melting than those of the ilmenite clinopyroxenites.

The sources of the ijolites and nepheline syenites have incompatible-element patterns close to those of OIB and are characterized by the highest $(^{87}Sr/^{86}Sr)_0$ ratios (0.703462–0.704144). The carbonatites are genetically related to the nepheline syenite melts according to the complementary distribution of incompatible elements and to the perovskite and ilmenite clinopyroxenites according to the range of $(^{87}Sr/^{86}Sr)_0$ = 0.7029–0.7034. The carbonatites could be formed by the immiscible-liquid or fluid segregation of melts from the ijolite–nepheline syenite source in the process of their interaction with the source of the perovskite and ilmenite clinopyroxenites.

ACKNOWLEDGMENTS

This study was financially supported by the Russian Foundation for Basic Research, project no. 05-05-64393.

REFERENCES

1. L. N. Kogarko, "Role of Sulfide–Carbonate–Silicate and Carbonate–Silicate Liquid Immiscibility in the Genesis of Ca-Carbonatites," in *Proceedings of International Conference on Deep-Seated Magmatism and Problems of Plume* (Irkutsk. Gos. Tekhn. Univ., Irkutsk, 2002), pp. 43–53 [in Russian].
2. K. Bell and A. Simonetti, "Carbonatite Magmatism and Plume Activity: Implications from the Nd, Pb and Sr Isotope Systematics of Oldoinyo Lengai," J. Petrol. **37**, 1321–1339 (1996).
3. A. A. Konev, *Zhidoi Alkaline–Ultrabasic Pluton* (Nauka, Moscow, 1970) [in Russian].
4. A. A. Konev, *Nepheline Rocks of the Sayan–Baikal Mountainous Area* (Nauka, Novosibirsk, 1982) [in Russian].
5. N. V. Vladykin, T. Morikiyo, T. I. Miyazaki, et al., "Geochemistry of Carbon and Oxygen Isotopes in the Siberian and Mongolian Carbonatites and Some Geodynamic Implications," in *Proceedings of the 4th International Seminar on Deep-seated Magmatism, its Sources, and their Relation with Plume Processes, Ulan Ude, Russia, 2004* (Inst. Geogr. Sib. Otd. RAN, Irkutsk, 2004), pp. 89–106 [in Russian].
6. T. Morikiyo, K. Takano, T. I. Miyazaki, et al., "Sr, Nd, S and O isotopic Compositions of Carbonatite and Peralkaline Silicate Rocks from the Zhidoy Complex, Russia," J. Mineral. Petrol. Sci. **95**, (162–172) 2000.
7. Yu. A. Bagdasarov, S. N. Voronezhskii, L. V. Ovchinnikova, et al., "New K–Ar Age Data on Ultramafic Alkaline Carbonatite Massifs of the Eastern Sayan and Some Problems of Their Formation," Dokl. Akad. Nauk **254** (1), 171–179 (1980).
8. N. A. Logachev, I. S. Brandt, S. V. Rasskazov, et al., "K–Ar Dating of the Paleocene Weathering Crust in the Baikal Region," Dokl. Akad. Nauk **385**, 797–799 (2002) [Dokl. Earth Sci. **385**, 648–650 (2002)].
9. A. V. Ivanov, S. V. Rasskazov, A. A. Konev, et al., "Melting of the Carbonated Mantle at the Vendian–Cambrian Boundary beneath the Margin of the Siberian Craton as Provoked by Removed Tectonic Processes: The Zadoi and Belaya Zima Complexes," in *Geology, Geochemistry, and Geophysics: Proceedings of All-Russia Scientific Conference of Russian Foundation for basic Research 10th Anniversary* (IZK SO RAN, Irkutsk, 2002), pp. 252–254 [in Russian].
10. E. A. Chernysheva, G. P. Sandimirova, Yu. A. Pakhol'chenko, et al., "Rb–Sr Age and Some Genetic Features of the Bol'-shaya Tagna Carbonatite Complex, Eastern Sayan,," Dokl. Akad. Nauk **323** (5), 942–948 (1992).
11. B. M. Vladimirov, N. A. Logachev, G. A. Vainer-Krotova, et al., " The Vendian–Cambrian Boundary: Rb–Sr Isochron Age of the Final Event of Alkaline Ultrabasic Magmatism in the Northeastern Sayan Region," Dokl. Akad. Nauk **389** (6), 777–780 (2003) [Dokl. Earth Sci. **389**, 346–349 (2003)].
12. S. A. Bowring, J. Ramezani, and J. P. Grotzinger, "High-Precision U–Pb Zircon Geochronology and the Cambrian–Precambrian Boundary," in *Proceedings of NUNA Conference of New Frontiers in the Fourth Dimension: Generation, Calibration and Application of Geological Timescales, Quebec, Canada, 2003*, (Quebec, 2003).
13. S.-S. Sun and W. F. McDonough, "Chemical and Isotopic Systematics of Oceanic Basalts: Implications for Mantle Composition and Processes," in *Magmatism in the Ocean Basins*, Ed. by A. D. Sounders and M. J. Norry, Geol. Soc. Spec. Publ. No. 42, 313–345 (1989).
14. D. M. Shaw, "Trace Element Fractionation during Anatexis," Geochim. Cosmochim. Acta **34**, 237–243 (1970).
15. N. W. Rogers, C. J. Hawkesworth, and Z. A. Palacz, "Phlogopite in the Generation of Olivine–Melilitites from Namaqualand," Lithos, 347–365 (1992).
16. Y. Tatsumi, R. Aral, and K. Ishizaka, "The Petrology of a Melilite–Olivine Nephelinite from Hamada, SW Japan," J. Petrol. **40** (4), 497–509 (1999).